Resolution Depths for Some Transmitter Receiver Configurations

J Torquil Smith, H Frank Morrison, Alex Becker
Lawrence Berkeley National Laboratory
Berkeley, California 94720

ABSTRACT

Equivalent dipole polarizability matrices and equivalent dipole location are a convenient way to interpret magnetic field data due to currents induced in isolated conductive objects. The uncertainties in polarizability estimates and in equivalent dipole location provide a quantitative measure of the performance of different configurations of transmitters and receivers. These uncertainties are estimated using a linearized inversion (Smith and Morrison, 2002). For many systems, consisting of one or more rectangular loop transmitters and a number of dipole receivers, sited on a horizontal grid, equivalent dipole depth is determined to 10% accuracy to depths approximately 20% deeper, than the depths at which polarizability matrix elements can be determined to the same precision. Systems that have a lower product of rms polarizability uncertainty and square root of their number of transmitter-receiver pairs are considered more effective for the number of transmitter-receiver pairs. Among the systems studied, a system with three orthogonal transmitter loops and a three component receiver is the most effective, for objects shallower than 0.6 times the instrument siting grid spacing, yielding an rms polarizability uncertainty 0.04 times that of a single transmitter single receiver system. At intermediate depths, a system with two vertical component receivers on the diagonal of a square horizontal transmitter loop is most effective for its number of transmitter-receiver pairs, yielding an rms polarizability uncertainty 0.07 times that of a single receiver system. At depths greater than 2.5 times the siting grid spacing a 3 orthogonal loop transmitter with a single vertical component receiver is about the most effective for its number of transmitter-receiver pairs, yielding an rms polarizability uncertainty 0.08 times that of a single transmitter system.

INTRODUCTION

Equivalent dipoles have long been used for approximating potential field sources in geophysics, as well as in other disciplines, and we will not attempt to outline the history of their usage. Recently, they have been used to model secondary magnetic fields arising from currents induced in isolated conductive, and possibly magnetic bodies, for location and identification of unexploded ordnance (UXO) by Khadr *et al*. (1998), Bell *et al*. (2001), Pasion and Oldenburg (2001), and Baum (1999), among others. In these recent examples, the amplitudes of induced dipoles are modelled as linearly proportional to the inducing magnetic fields at the body centers and related to them by equivalent dipole polarizability matrices.

Equivalent dipole polarizability matrices and dipole locations are a convenient way to summarize active source induced current magnetic field measurements in an interpretable form. The matrices' principal moments give information on the rotational symmetry of a conductive object, their principal directions yield the object's orientation, and the dipole location $\mathbf{r}_o$ estimates the object's center position. Smith and Morrison (2002) ("paper I") give a very clear treatment of an algorithm for estimating the equivalent dipole polarizability matrix and equivalent dipole position, with explicit expressions for uncertainties in the estimated quantities. Here the uncertainty estimates are used to compute the depths to which the polarizability matrices and dipole locations can be estimated for steel spheres of varying radius, for several transmitter-receiver configurations.

EQUIVALENT DIPOLE POLARIZABILITY MATRICES

Equivalent dipole polarizability matrices **M** are used to model observed secondary magnetic fields $\mathbf{B}^{(s)}(\mathbf{r},t)$, in terms of the magnetic fields of unit dipoles in the $\hat{\mathbf{x}}$, $\hat{\mathbf{y}}$, and $\hat{\mathbf{z}}$ directions, $\mathbf{B}_x^{(d)}(\mathbf{r})$, $\mathbf{B}_y^{(d)}(\mathbf{r})$, $\mathbf{B}_z^{(d)}(\mathbf{r})$, centered at some location $\mathbf{r}_o$, and a nominal primary (inducing) magnetic field strength $\mathbf{B}^{(o)}$ at $\mathbf{r}_o$,

$$\mathbf{B}^{(s)}(\mathbf{r},t) = \left[\mathbf{B}_x^{(d)}(\mathbf{r}), \mathbf{B}_y^{(d)}(\mathbf{r}), \mathbf{B}_z^{(d)}(\mathbf{r})\right] \; \mathbf{M}(t) \; \mathbf{B}^{(o)} \quad , \tag{1}$$

for a given time variation $g(t)$ of primary magnetic field, $g(t)\,\mathbf{B}^{(o)}$, such as a unit

step function turn-off. In this model, the polarizability matrix is independent of transmitter and receiver geometry and object location, depending only on the innate properties of the object, its orientation, and the transmitter wave form. The principal values of **M**, depend only on the object, independent of its orientation, and on the transmitter waveform. Equivalent dipole position $\mathbf{r}_o$ is generally assumed to coincide with the object center.

For typical time domain systems, secondary fields are measured after primary fields are extinct, at which time the entire magnetic field is secondary. In simplest form, the time variation of the primary field is incorporated in the estimated polarizability matrix $\mathbf{M}(t)$, and the primary magnetic field strength vector at object center $\mathbf{B}^{(o)}$, for a given source, is simply the magnetic field there for a D.C. current in the transmitter coils of the transmitter's nominal current strength (e.g, peak current strength). For modeling magnetic field time derivative data, the same model is applicable with $d\mathbf{B}^{(s)}(\mathbf{r},t)/dt$ replacing $\mathbf{B}^{(s)}(\mathbf{r},t)$, and $d\mathbf{M}(t)/dt$ replacing $\mathbf{M}(t)$ in equation (1).

When the equivalent dipole position $\mathbf{r}_o$ is known, secondary magnetic field values depend linearly on the unknown polarizability matrix **M**, that may be estimated by minimizing the misfit to secondary magnetic field observations (data) for primary fields with at least three linearly independent orientations $\mathbf{B}^{(o)}$ at the equivalent dipole location. When the equivalent dipole position is unknown, the same procedure may be used at a series of candidate equivalent dipole positions, calculating the minimum data misfit attainable for each candidate position, and some search strategy used to find the position with lowest attainable data misfit.

Once the lowest attainable data misfit has been found, uncertainties in the resultant polarizability matrix and equivalent dipole location may be estimated from the partial derivatives of the observed data with respect to the model parameters. Paper I gives equations for the uncertainties in detail. These uncertainty estimates are based on a perturbation analysis and are strictly accurate in the limit of small observation errors.

METHOD

The methods of paper I were used to estimate equivalent dipole polarizabilities from synthetic three component magnetic field data measured coincident with a vertical magnetic dipole source at 13 sites placed symmetrically on a rectangular grid above steel spheres of varying radius, modelled with a conductivity of $\sigma = 10^7\ \Omega^{-1}m^{-1}$ and relative permeability $\mu_r = 180$. Spheres smaller than 0.1 m radius were placed at 1 m depth below the center of the grid. Spheres larger than 0.1 m radius were placed at a depth of ten radii. The siting grid had 0.4 m spacings in x and y for all but the largest sphere, for which the grid spacing was 5 m. A step function turn-off transmitter current was used, as the most generic of waveforms, and an observation time of 610 μs after turnoff chosen to simulate the effective center time of the averaging gate of an existent commercial transmitter-receiver system. Polarizability estimates are listed in Table 1. In principle, for spherically symmetric objects, the three principal moments are identical. The variation between estimated principal moments is less than 1% for spheres smaller than 25 cm radius. The variations are due to the limited spatial extent of the data used, the presence of non-dipole moment components in the data, and truncation of the data at four significant figures. In subsequent computations based on Table I, the three estimated moments were replaced with their average.

Paper I gives equations for the covariance matrix for dipole polarizability matrix **M** elements, and covariance matrices for the principal moments and directions derived from it. In general, computing principal moments and directions requires knowing all elements of **M** (which is symmetric). If principal directions are known *a priori*, principal moments may be determined from fewer measurements, but determining the principal directions empirically requires knowledge of all elements of **M**. A simple measure of how well a data set resolves **M** is the total squared uncertainty

$$\varepsilon^2 \equiv \sum_{i=1}^{3} \sum_{j=1}^{3} var(m_{ij}) \quad , \tag{2}$$

where $var(m_{ij})$ is the estimated squared uncertainty of the ij'th element of **M**

obtained from the diagonal of the covariance matrix of the elements of **M** ($cov(\mathbf{m})$ of paper I). The sum of the squares of the elements of a matrix is a matrix invariant, independent of the coordinates used to express **M**. In our experience, ε^2 is also independent of the coordinates used to express **M**. It is also convenient to define the relative uncertainty in polarizability, ξ;

$$\xi^2 \equiv \sum_{i=1}^{3}\sum_{j=1}^{3} var(m_{ij}) \;/\; \sum_{i=1}^{3}\sum_{j=1}^{3} m_{ij}^2 \quad . \tag{3}$$

Estimates of the variance in polarizabilities $var(m_{ij})$ based on inversion of a single set of noisy data, depend on the specific values (realization) of noise in the data, through the use of the partial derivatives of the data with respect to model parameters evaluated at the minimum of data misfit for that noise realization, in place of the partial derivatives evaluated at the true parameter values. As noted in Paper I, in evaluating system performance by inversion of synthetic data, one can eliminate the dependence of variance estimates on noise realization, by using partial derivatives evaluated at the true parameter values, resulting in a parameter covariance matrix estimate $\overline{cov}(\tilde{\mathbf{m}})$ with parameter variance estimates $\overline{var}(m_{ij})$ on its diagonal. All quantities plotted in the current paper are based on variance estimates of this type. Being independent of the specific noise realization, these estimates are entirely reproducible, as they do not depend on the particular seed used to start a sequence of random numbers which simulate noise in data.

As noted in paper I, for a given transmitter-receiver configuration, the size of uncertainty estimates in polarizability based on $\overline{cov}(\tilde{\mathbf{m}})$ is independent of the scale of the polarizability matrix of the target object. This means that for a given instrumental configuration one need only calculate polarizability moment uncertainties once for any particular ratios of principal polarizabilities, orientation of principal directions, and object position, and all other objects with the same ratios of principal moments, orientation, and position will have the same expected moment uncertainties. For spheres, which are isotropic, one need only calculate moment uncertainties once for a given location of sphere relative to the instrument configuration. Similarly, the size of

uncertainty estimates for equivalent dipole location scale inversely with the target polarizability matrix.

For each of a number of transmitter-receiver configurations, the total uncertainty ε was computed as a function of sphere depth, for spheres directly below the center of a 9x9 grid of system placements with 0.4 m spacing in x and y. One meter square transmitter loops were used with a moment of 180 Amp-m^2, and a receiver noise level of 1.97 nT/s in vertical field measurements, simulating an observed noise level, and 5.91 nT/s in horizontal field components (when present) simulating the larger noise levels observed in horizontal components.

RESULTS

Uncertainties in the diagonal elements of the polarizability matrix $d\mathbf{M}/dt$ are plotted in Figure (1) as a function of depth below transmitter and receiver, together with the total uncertainty ε, for isotropic equivalent dipole polarizabilities (spheres) below the grid of system placements for a horizontal loop transmitter/concentric vertical magnetic dipole receiver system. Being based on a linearized inversion for $d\mathbf{M}/dt$ and $\mathbf{r}_o$, these uncertainty estimates scale linearly with receiver noise level. The total moment uncertainty ε reaches a minimum near a depth of 0.14 meters. For shallower spheres, the uncertainties in dm_{xx}/dt, dm_{yy}/dt, and off diagonals dm_{xy}/dt, dm_{yz}/dt, dm_{xz}/dt (not shown) increase greatly approaching the plane of the transmitter and receiver, as all the transmitter placements illuminate the sphere with nearly vertical primary fields, yielding less information on these moments, and correspondingly large variances in them. The rise in all uncertainties below 0.18 m depth, reflects the decrease of primary field strengths with increasing depth. Below 1.5 m depth the uncertainty rises faster than z^6, implying that at these depths the loss of resolution is also due to the limited aperture of the 3.2 m by 3.2 m system placement (sampling) grid. The great increase of uncertainty with depth for spheres at large depths limits the depths for which polarizabilities can be resolved. Comparing the plotted values with the 610 μs polarizabilities of steel spheres of various radii, which are indicated on the left, the total uncertainty at shallow depths is considerably smaller than all indicated sphere polarizabilities. Since spheres have three equal principal moments, one can easily

convert the total uncertainty ε to relative uncertainty ξ, by dividing by $\sqrt{3}$ times the indicated polarizabilities. For a 6 cm radius steel sphere at 610 μs the relative uncertainty ξ reaches 0.1 (10%) at 1.47 m depth. The corresponding relative uncertainties in horizontal and vertical polarizabilities are 0.061, 0.061, and 0.147 respectively.

Uncertainties in location depend on the scale of the polarizability matrix, so must be calculated for specific objects. Relative uncertainties in vertical location and horizontal location are plotted as a function of depth below transmitter and receiver in Figure (2), for an isotropic polarizability corresponding to a 6 cm radius steel sphere at 610 μs, for the same transmitter-receiver system as in Figure (1), on the same grid of system placements. These uncertainties can be scaled to correspond to other radius spheres by dividing by the ratio of polarizabilities of the spheres. Both horizontal and vertical uncertainties have been normalized by the depth to the equivalent dipoles. Because of symmetry of the transmitter and receiver, and of the sampling grid, uncertainties in x and y are identical. The large increase in uncertainty in x and y at very small depths is not a substantial problem as transmitter-receiver systems are typically raised a small amount above the ground. As with the polarizability uncertainties, the great increase of location uncertainties for spheres at large depths limits the depths for which location, particularly depth, can be resolved. The relative uncertainty in depth reaches a 0.1 (10%) level by 1.83 m depth.

Because of the great range in the size of uncertainties in both equivalent dipole polarizability and location, it can be difficult to see differences in uncertainties when comparing plots for different transmitter-receiver systems. For comparison purposes, it is convenient to plot the depth to some level of relative uncertainty for isotropic polarizabilities corresponding to spheres of varying radius. Using the total uncertainties shown in Figure (1), depths to 5, 10, and 20% (rms) uncertainty in polarizability $d_{5\%}^{(p)}$, $d_{10\%}^{(p)}$, and $d_{20\%}^{(p)}$, were found for isotropic polarizabilities corresponding to the spheres in Table I, and are plotted in Figure (3), as a function of sphere radius. Similarly, the results of Figure (2) were scaled for the various spheres of Table I, and the depths to 5, 10, and 20% uncertainty in estimated sphere depth, $d_{5\%}^{(z)}$, $d_{10\%}^{(z)}$, and $d_{20\%}^{(z)}$, calculated, and are plotted in Figure (4). In general, object position can be estimated more

precisely than the full polarizability matrix, as object position may be determined when an object is illuminated by only a single orientation of primary field, whereas estimating the full polarizability matrix requires illuminating the object with primary fields $\mathbf{B}_o$ in at least three directions, each with a significant component in the direction orthogonal to the other two. Consequently, object depth can be resolved within 10% to greater depths than polarizability in all cases plotted. The relative uncertainties in polarizability and position depend on all elements of the polarizability matrix **M** (through $\tilde{\mathbf{F}}$, $\mathbf{g}_i^{(q)}$, and $m_{kj}^{(q)}$ of paper I), depending on both its principal values, and principal directions (object orientation). Most cases presented here are for spherical objects, for which the principal values are all the same, and the polarizability **M** is coordinate independent. For comparison $d_{10\%}^{(p)}$ and $d_{10\%}^{(z)}$ are plotted in Figure (5) for the same transmitter-receiver pair, for the case of objects with the same vertical dipole polarizability dm_{zz}/dt at 610 μs as the spheres of Table I, and all other polarizabilities null, corresponding to thin horizontal non-magnetic discs. The general trends are the same as for the sphere. Polarizability can be resolved to 10% slightly deeper than for the sphere for all but the 1 cm radius. Object depth can be resolved approximately 1.2 times deeper than for the sphere.

Effects of adding a second coaxial vertical receiver 0.4 m above the first are shown in Figure (6), where $d_{10\%}^{(p)}$ and where $d_{10\%}^{(z)}$ are plotted for the two receiver system (solid) together with their values for the previously plotted single receiver system (dotted). In addition to resolving polarizabilities and location to greater depth as shown here, the added receiver makes locating the object position an easier problem as it eliminates a secondary minimum in data misfit near the true object position (paper I).

Figure (7) shows $d_{10\%}^{(p)}$ and $d_{10\%}^{(z)}$ (both solid) for a similar system with the two vertical component receivers in the plane of the transmitter loop, offset ±0.2 m in x and y along a diagonal from the loop center. This system shows greatest improvement in sensitivity over the single receiver system for objects close to the transmitter-receiver plane, greatly increasing the depths to which the smallest spheres can be

resolved.

Results for a horizontal loop transmitter with a three component concentric receiver are shown in Figure (8) (solid lines). For comparison, a system with a 1 m^2 horizontal loop and two orthogonal 1 m^2 vertical loop transmitters with lower edges at the level of the horizontal loop is shown in Figure (9) (solid lines). The results for the 3 transmitter 1 receiver system are substantially better than for the 1 transmitter 3 receiver system, in part, because of the greater noise level in horizontal component receivers.

As a final example, adding 2 orthogonal horizontal component receivers to the 3 transmitter system to make a 3 transmitter 3 receiver system yields results shown in Figure (10). The added horizontal components substantially increase the depth of resolution of the 1 cm radius sphere, but little affect results for 3 cm radius and larger spheres.

That adding more transmitter-receiver combinations to a system decreases uncertainties in the recovered object parameters, increasing the depths to which the polarizability matrix and equivalent dipole location can be recovered, is no surprise. When averaging n measurements of a single kind of data, uncertainty in the average decreases as $1/\sqrt{n}$, so one expects a decrease on the order of the reciprocal of the square root of the number of transmitter-receiver pairs $(n_r n_t)^{-½}$. To allow discerning which of the preceding systems resolves polarizability most effectively for its number of transmitter-receiver pairs, total moment uncertainty ε multipled by $(n_r n_t)^{½}$ is plotted in Figure (11) as a function of sphere depth. The differences between curves mean that adding transmitters or receivers can reduce the uncertainty in the polarizability matrix by substantially more than by the factor of $(n_r n_t)^{-½}$ that is to be expected solely from an increase in the number of data.

For spheres above 0.26 m depth, the system with most receiver-transmitter pairs close to the object (three orthogonal loop transmitters and a 3 component receiver), gives the lowest $\varepsilon \cdot (n_r n_t)^{½}$ product, achieving a moment uncertainty 22.8 times smaller than the single transmitter single receiver system for spheres at 0.1 m depth.

Between 0.26 to 1.0 m, as sphere depths become commensurate with the sampling grid spacing (0.4 m), the system with two vertical component receivers along the diagonal of the transmitter loop (of Figure 7) gives the lowest $\varepsilon \cdot (n_r n_t)^{1/2}$ product. At 0.5 m depth near where their ratio of uncertainties is greatest, the two vertical component receiver uncertainty is a factor of 13.6 times smaller than the single transmitter single receiver system uncertainty. Below 1.0 m the 3 orthogonal transmitter loop vertical component receiver (of Figure 9) gives the lowest $\varepsilon \cdot (n_r n_t)^{1/2}$ product; at 2.0 m depth, this system reduces the uncertainty by a factor of 11.8 compared to the single transmitter single receiver system. With the last system, adding additional vertical component receivers within the horizontal transmitter loop can result in $\varepsilon \cdot (n_r n_t)^{1/2}$ curves that are lower than the single receiver system curve at some depths, but in all cases that we have examined, the improvements in $\varepsilon \cdot (n_r n_t)^{1/2}$ between 1 m and 5 m are fairly marginal. For example, adding a receiver at one of the horizontal loop corners reduces ε by a factor of 1.46 for spheres at 2 meters depth, rather than the $\sqrt{2}$ factor expected due to doubling the number of data, or, substituting vertical component receivers at two opposite corners for the single receiver at the horizontal loop center, reduces the uncertainty by a factor of 1.57 for spheres at 5 m depth, but only by a factor of 1.37 for spheres at 2 m depth, compared to the three transmitter single receiver system.

CONCLUSION

The polarizability matrix **M** and equivalent dipole polarizability location are best determined for objects at depths on the order of the system placement grid spacing or less. Determining all elements of the polarizability matrix **M**, to be able to compute its principal components, is a more demanding task than determining equivalent dipole polarizability location. For the transmitter-receiver combinations studied here, one can determine the equivalent dipole depth to within 10 % approximately 20 % deeper than one can determine the polarizability matrix to the same precision. Adding additional sources or receivers can improve the resolving power of a single transmitter single receiver system, by factors substantially better than the simple reduction by $(n_r n_t)^{-1/2}$ due to the increased number of data. Adding transmitter loops orthogonal to a horizontal

transmitter loop is more effective than adding receiver components orthogonal to a vertical component receiver, as vertical component receivers generally have less noise than horizontal component receivers. For objects a few times deeper than the sampling grid spacing, a 3 orthogonal-transmitter loop, single vertical component receiver system is about the most effective for its number of receiver-transmitter pairs. Adding additional vertical component receivers to such a system reduces the uncertainty in **M**, by about the amount expected for averaging of an increased number of data, $(n_r n_t)^{-½}$. For objects shallower than the sampling grid spacing, adding additional receivers and transmitter polarizations both can substantially improve the precision of polarizability matrix and dipole location estimates.

ACKNOWLEDGEMENT

This work was supported by the US Department of the Army under Contract No. W74RDV93447299.

REFERENCES

C. E. Baum, ‘‘Low frequency near-field magnetic scattering from highly conducting, but not perfectly conducting bodies,’’ in C. E. Baum, Ed., *Detection and Identification of Visually Obscured Targets,* Philadelphia: Taylor et Francis, ch. 6, pp. 163-217, 1999.

T. H. Bell, B. J. Barrow, and J. T. Miller, ‘‘Subsurface discrimination using electromagnetic induction sensors,’’ *IEEE Trans. Geosci. Remote Sensing,* vol. 39, no. 6, pp. 1286-1293. June 2001.

N. Khadr, B. J. Barrow, T. H. Bell, and H. H. Nelson, ‘‘Target shape classification using electromagnetic induction sensor data,’’ in *Proceeding of UXO Forum* 1998.

L. R. Pasion and D. W. Oldenburg, ‘‘Locating and determining dimensionality of UXOs using time domain electromagnetic fields,’’ *Journal of Environmental and Engineering Geophysics*, vol. 6, no. 2, pp. 91-102, June 2001.

J. T. Smith and H. F. Morrison, ‘‘Estimating Equivalent Dipole Polarizabilities for the Inductive Response of Isolated Conductive Bodies,’’ to be submitted to *IEEE Trans. Geosci. Remote Sensing,* 2002.

FIGURE CAPTIONS

Figure (1). Total polarizability uncertainty ε (solid), as a function of sphere center depth below siting grid center, for a 1 m^2 square loop transmitter with a concentric vertical dipole receiver sited on a 9x9 grid with 0.4 m spacings. Also, uncertainty in vertical moment dm_{zz}/dt (dashed), and in horizontal moments dm_{xx}/dt and dm_{yy}/dt (dotted). Polarizabilities of steel spheres of various radii are indicted on left axis.

Figure (2). Relative uncertainty in equivalent dipole position, for a 0.641 Amp-m^2/s/μT isotropic polarizability as a function of depth below center of siting grid, for same system and grid as in Figure (1). Uncertainty in z (solid), uncertainty in x and y (dashed).

Figure (3). Depths to 5%, 10%, and 20% uncertainty in polarizability as a function of sphere radius for steel spheres, for same system and grid as in Figure (1).

Figure (4). Depths to 5%, 10%, and 20% uncertainty in sphere center depth, as a function of sphere radius for steel spheres, for same system and grid as in Figure (1).

Figure (5). Depths to 10% polarizability uncertainty and to 10% uncertainty in center depth, for thin horizontal non-magnetic disk with same vertical polarizability dm_{zz}/dt at 610 μs, as spheres of Table I, plotted as a function of the corresponding sphere's radius, for same system and grid as in Figure (1).

Figure (6). Depths to 10% polarizability uncertainty and to 10% uncertainty in center depth, as a function of radius for steel spheres below a 1 m^2 square transmitter loop with two coaxial vertical component receivers 0.4 m apart vertically, on same grid as in Figure (1).

Figure (7). Depths to 10% polarizability uncertainty and to 10% uncertainty in center depth, as a function of sphere radius, for 1 m^2 loop transmitter system with two vertical component receivers 0.566 m apart on diagonal in plane of transmitter loop, on same grid as in Figure (1).

Figure (8). Depths to 10% polarizability uncertainty and to 10% uncertainty in depth as a function of sphere radius, for 1 m^2 loop transmitter system with 3 component concentric receiver, on same grid as in Figure (1).

Figure (9). Depths to 10% polarizability uncertainty and to 10% uncertainty in depth, as a function of sphere radius, for three orthogonal 1 m^2 loop transmitter system with vertical component receiver at horizontal loop center, on same grid as in Figure (1).

Figure (10). Depths to 10% polarizability uncertainty and to 10% uncertainty in depth, as a function of sphere radius, for 3 transmitter loop system with 3 component receiver at horizontal loop center, on same grid as in Figure (1).

Figure (11). Total polarizability uncertainty ε divided by expected improvement $(n_r n_t)^{-½}$ due increase in number of data, as a function of sphere center depth below center of system siting grid. (Solid) system of Figures (1)-(5). (Long dashes) system of Figure (8). (Medium dashes) system of Figure (10). (Dashed-dotted) system of Figure (6). (Dotted) system of Figure (9). (Short dashes) system of Figure (7).

Table I. Estimated principal moments for simulated steel sphere data at 610 μs after step function turn-off, from 13 vector measurements coincident with vertical dipole source on grid 1 m, or 10 radii, above sphere center.

Radius (m)	Estimated Principal Moments (Amp-m^2/s/T)		
0.01	$-7.28\ 10^2$	$-7.28\ 10^2$	$-7.28\ 10^2$
0.02	$-1.11\ 10^4$	$-1.11\ 10^4$	$-1.11\ 10^4$
0.03	$-5.26\ 10^4$	$-5.26\ 10^4$	$-5.26\ 10^4$
0.04	$-1.53\ 10^5$	$-1.53\ 10^5$	$-1.53\ 10^5$
0.05	$-3.41\ 10^5$	$-3.41\ 10^5$	$-3.40\ 10^5$
0.06	$-6.42\ 10^5$	$-6.42\ 10^5$	$-6.40\ 10^5$
0.08	$-1.67\ 10^6$	$-1.67\ 10^6$	$-1.66\ 10^6$
0.10	$-3.38\ 10^6$	$-3.38\ 10^6$	$-3.36\ 10^6$
0.15	$-1.12\ 10^7$	$-1.12\ 10^7$	$-1.11\ 10^7$
0.25	$-4.42\ 10^7$	$-4.42\ 10^7$	$-4.37\ 10^7$
0.50	$-2.35\ 10^8$	$-2.35\ 10^8$	$-2.29\ 10^8$
1.00	$-1.10\ 10^9$	$-1.10\ 10^9$	$-1.09\ 10^9$

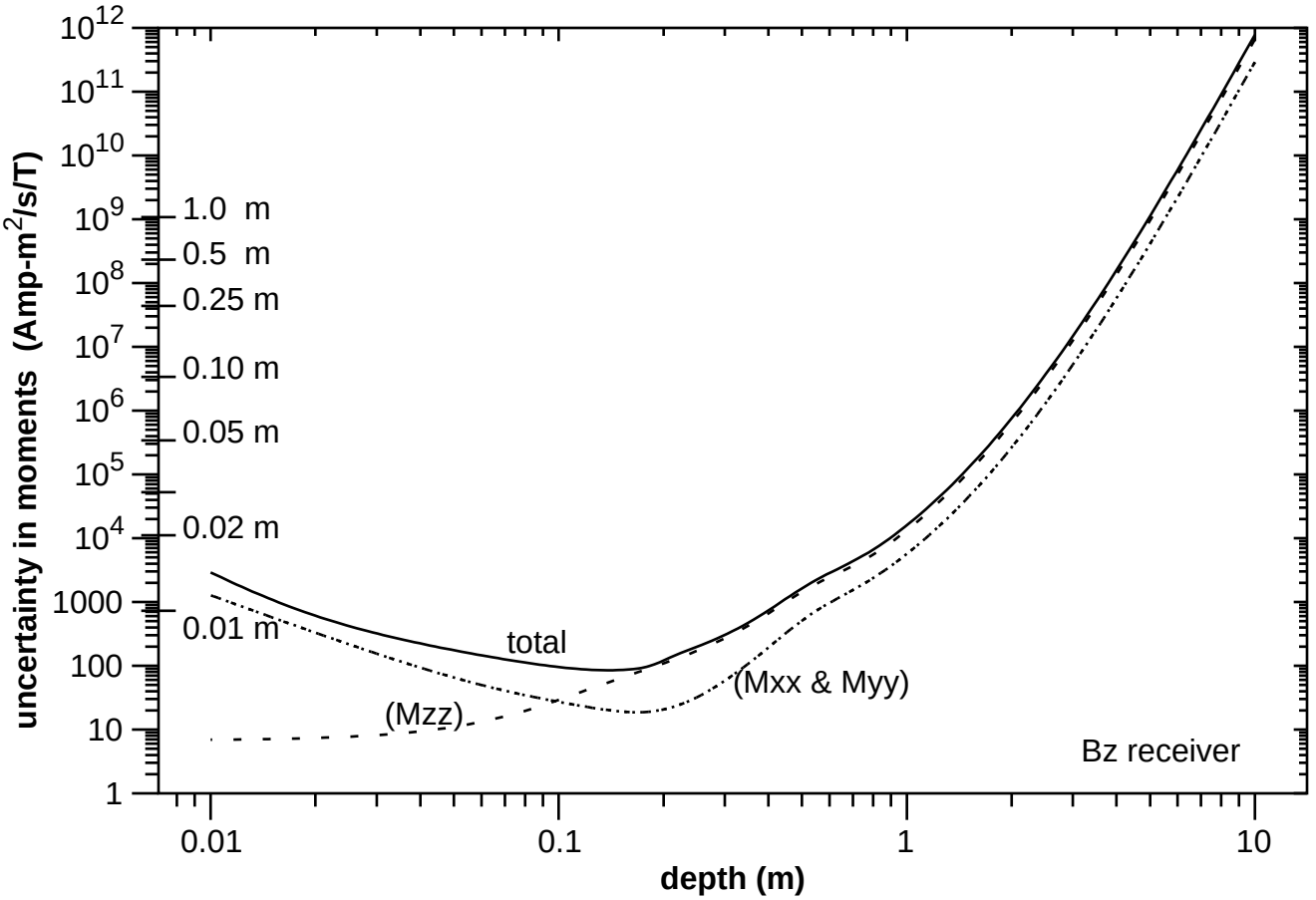
uncertainty in moments (Amp-m²/s/T)
10^12
10^11
10^10
10^9
10^8
10^7
10^6
10^5
10^4
1000
100
10
1
1.0 m
0.5 m
0.25 m
0.10 m
0.05 m
0.02 m
0.01 m
total
(Mxx & Myy)
(Mzz)
Bz receiver
0.01
0.1
1
10
depth (m)

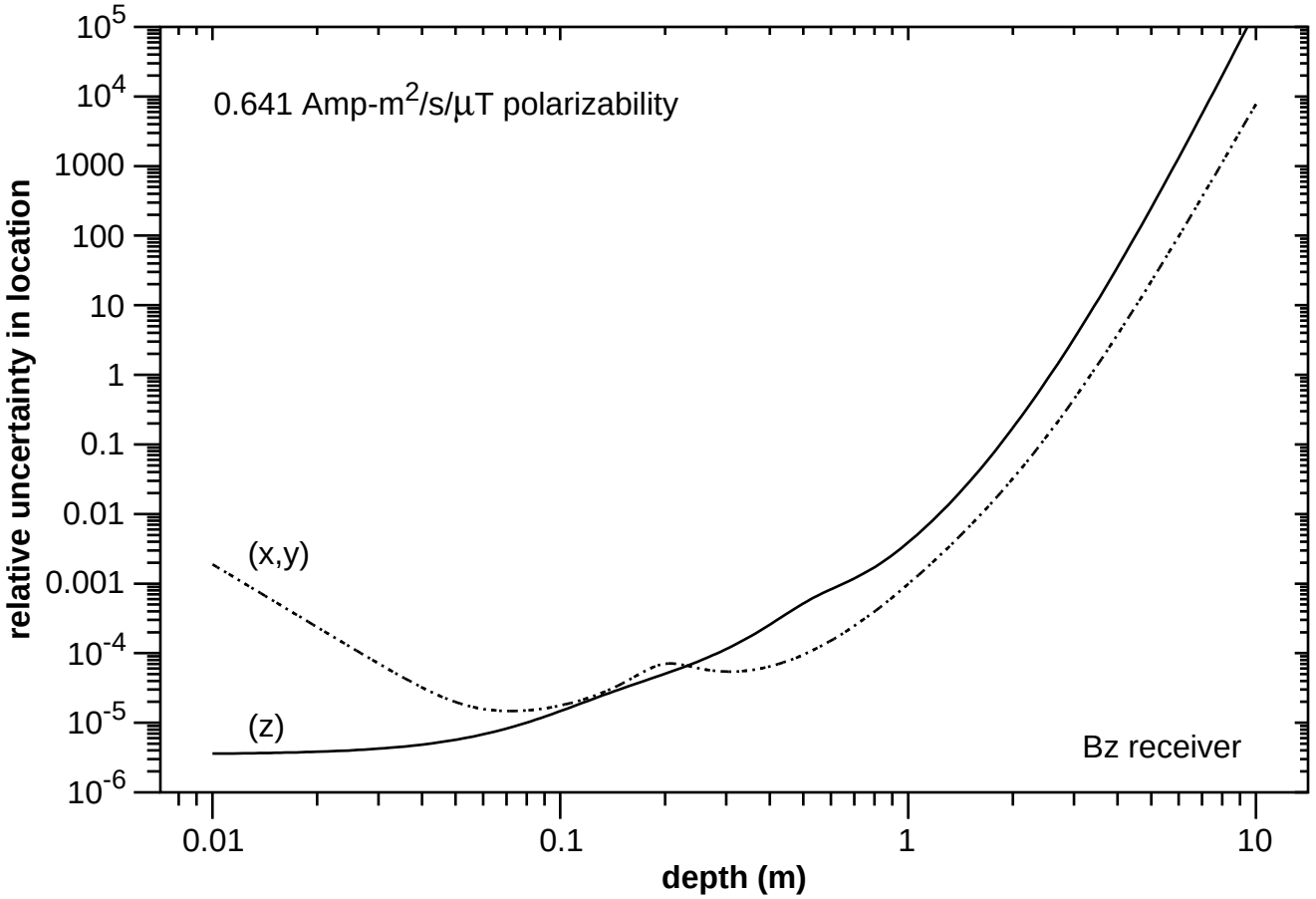
0.641 Amp-m2/s/μT polarizability
(x,y)
(z)
Bz receiver
relative uncertainty in location
depth (m)
10^5
10^4
1000
100
10
1
0.1
0.01
0.001
10^-4
10^-5
10^-6
0.01
0.1
1
10

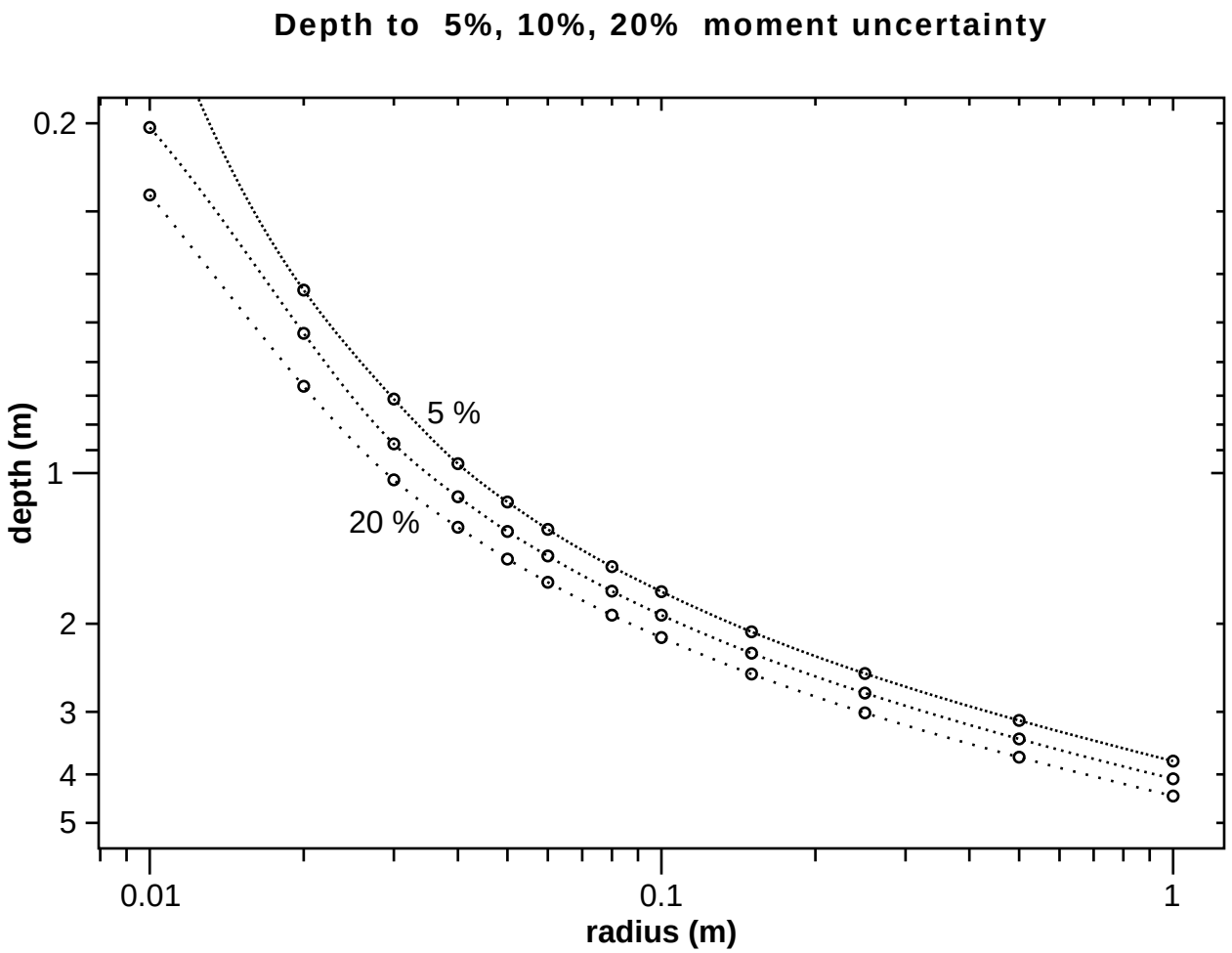
Depth to 5%, 10%, 20% moment uncertainty
0.2
1
2
3
4
5
depth (m)
5 %
20 %
0.01
0.1
1
radius (m)

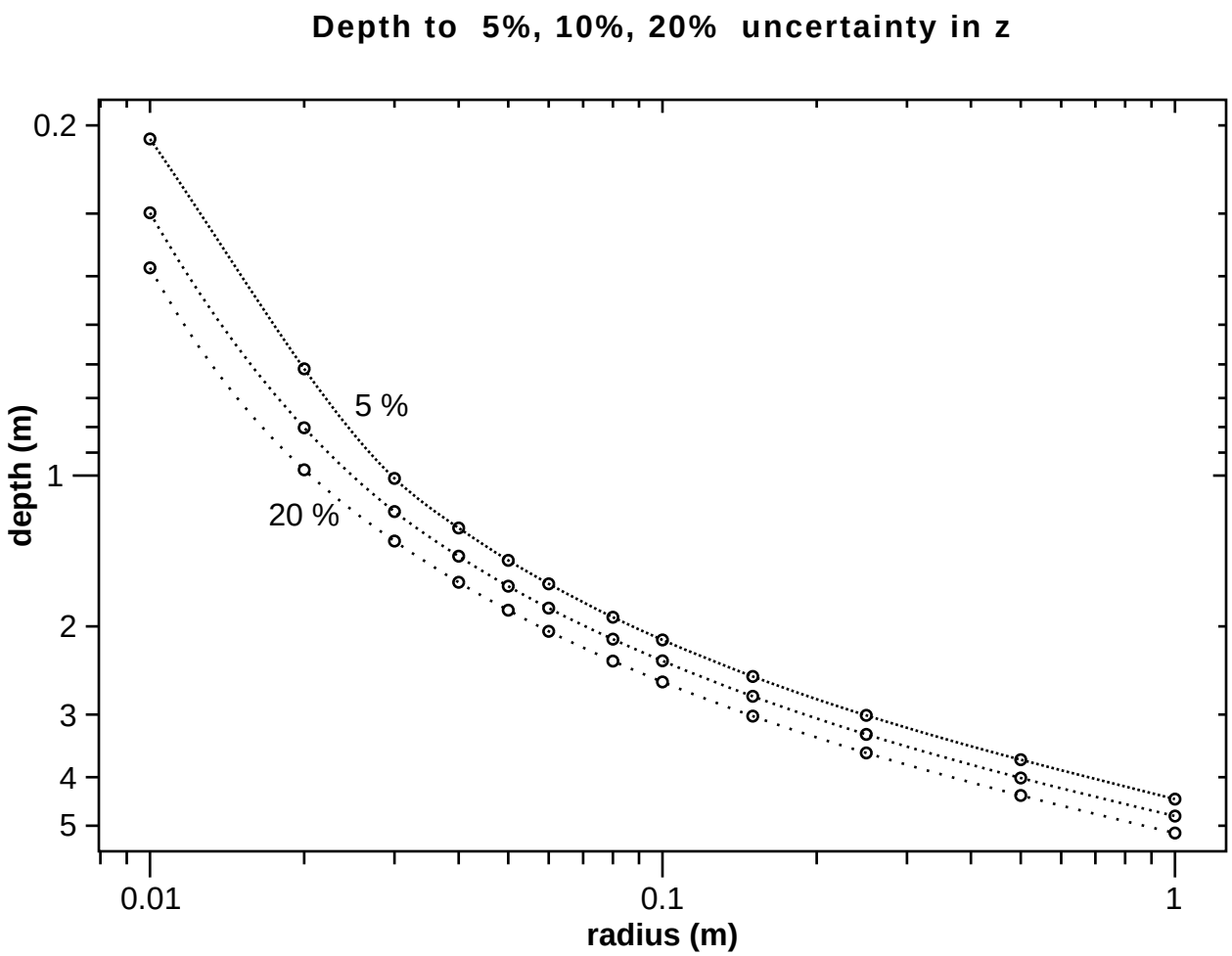
Depth to 5%, 10%, 20% uncertainty in z
0.2
1
2
3
4
5
depth (m)
5 %
20 %
0.01
0.1
1
radius (m)

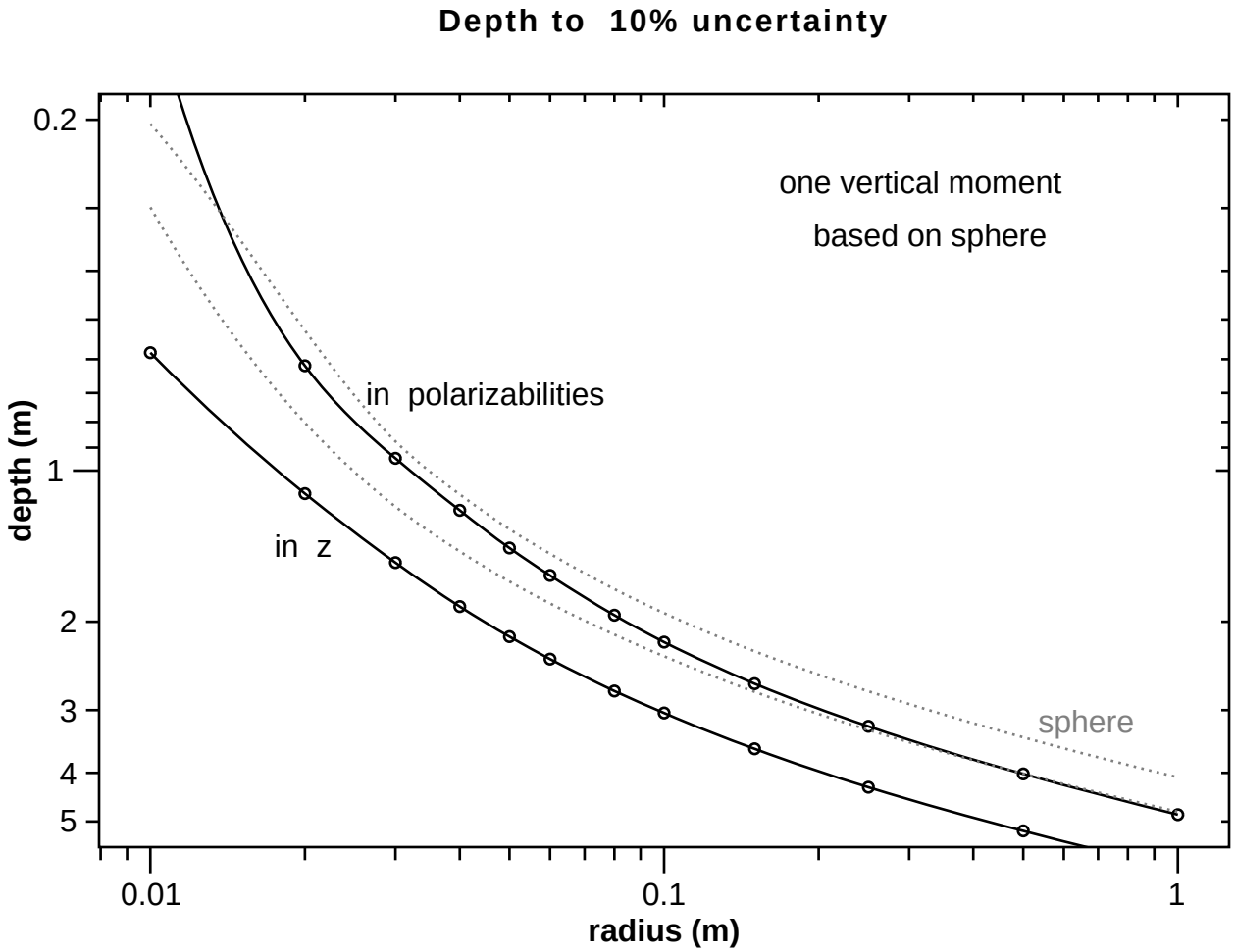
Depth to 10% uncertainty
0.2
1
2
3
4
5
depth (m)
0.01
0.1
1
radius (m)
one vertical moment
based on sphere
in polarizabilities
in z
sphere

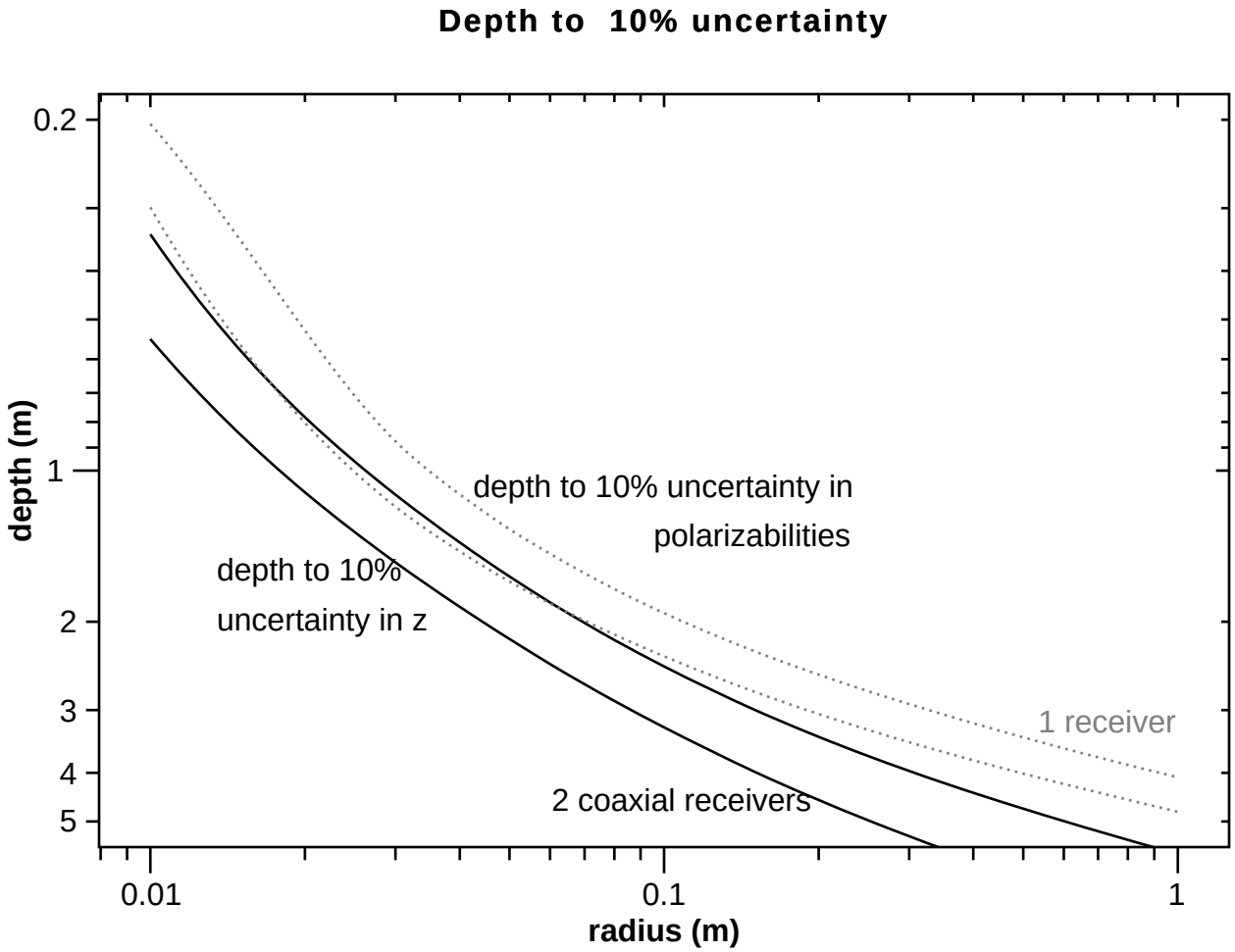
Depth to 10% uncertainty
0.2
1
2
3
4
5
depth (m)
0.01
0.1
1
radius (m)
depth to 10% uncertainty in
polarizabilities
depth to 10%
uncertainty in z
1 receiver
2 coaxial receivers

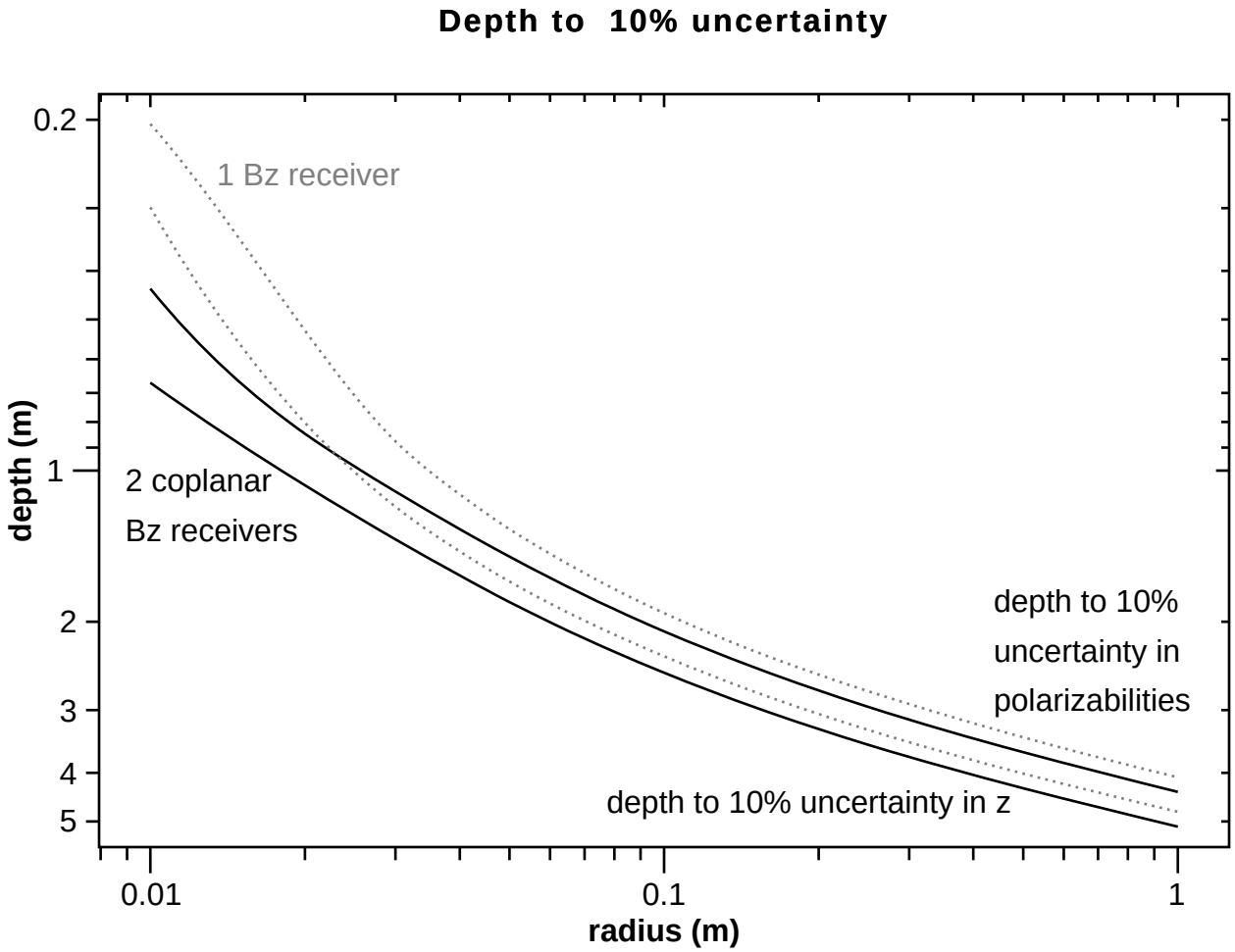
Depth to 10% uncertainty
0.2
1
2
3
4
5
depth (m)
1 Bz receiver
2 coplanar
Bz receivers
depth to 10%
uncertainty in
polarizabilities
depth to 10% uncertainty in z
0.01
0.1
1
radius (m)

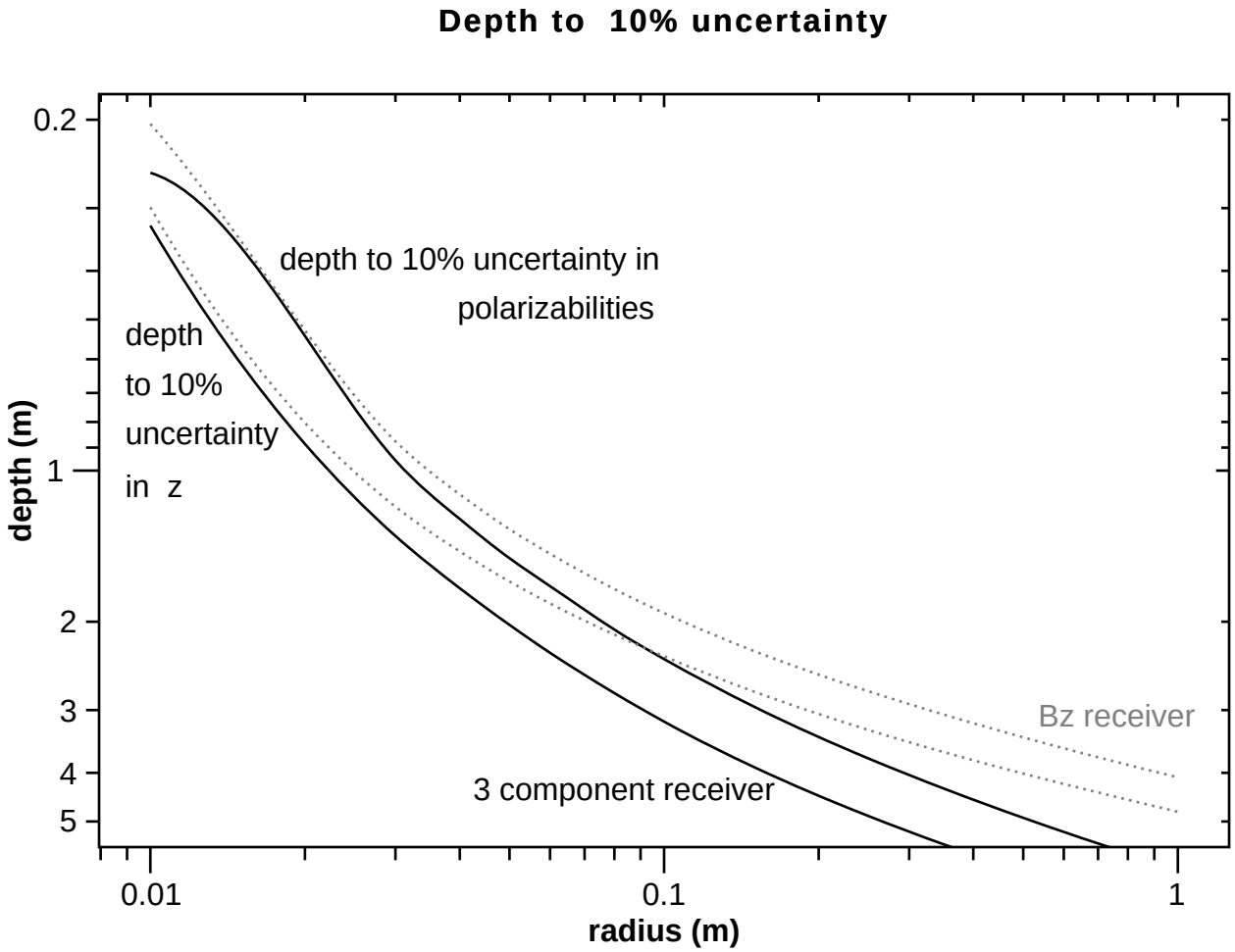
Depth to 10% uncertainty
0.2
1
2
3
4
5
depth (m)
0.01
0.1
1
radius (m)
depth to 10% uncertainty in
polarizabilities
depth
to 10%
uncertainty
in z
Bz receiver
3 component receiver

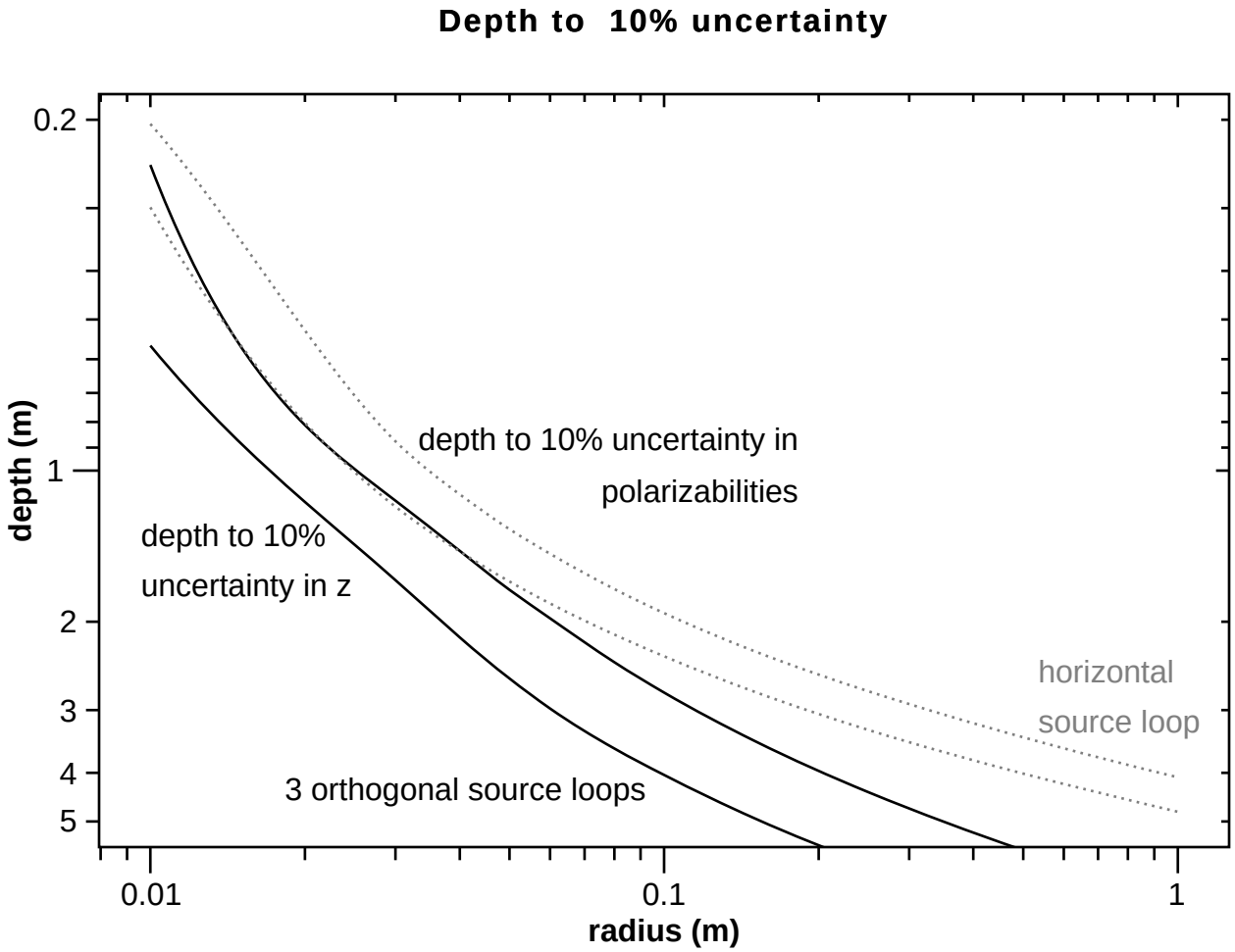
Depth to 10% uncertainty
depth (m)
0.2
1
2
3
4
5
0.01
0.1
1
radius (m)
depth to 10% uncertainty in
polarizabilities
depth to 10%
uncertainty in z
horizontal
source loop
3 orthogonal source loops

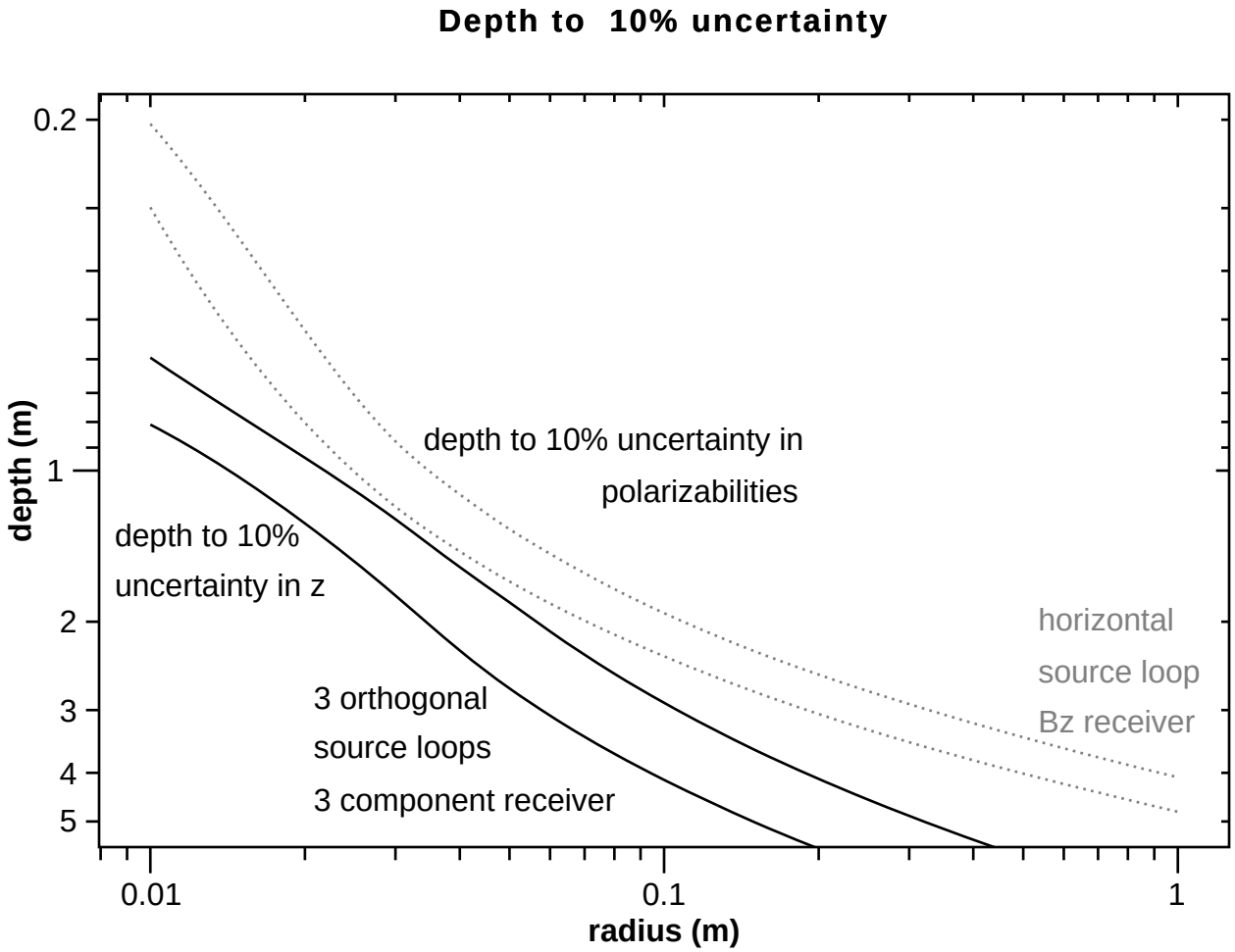
Depth to 10% uncertainty
0.2
1
2
3
4
5
depth (m)
0.01
0.1
1
radius (m)
depth to 10% uncertainty in
polarizabilities
depth to 10%
uncertainty in z
horizontal
source loop
Bz receiver
3 orthogonal
source loops
3 component receiver

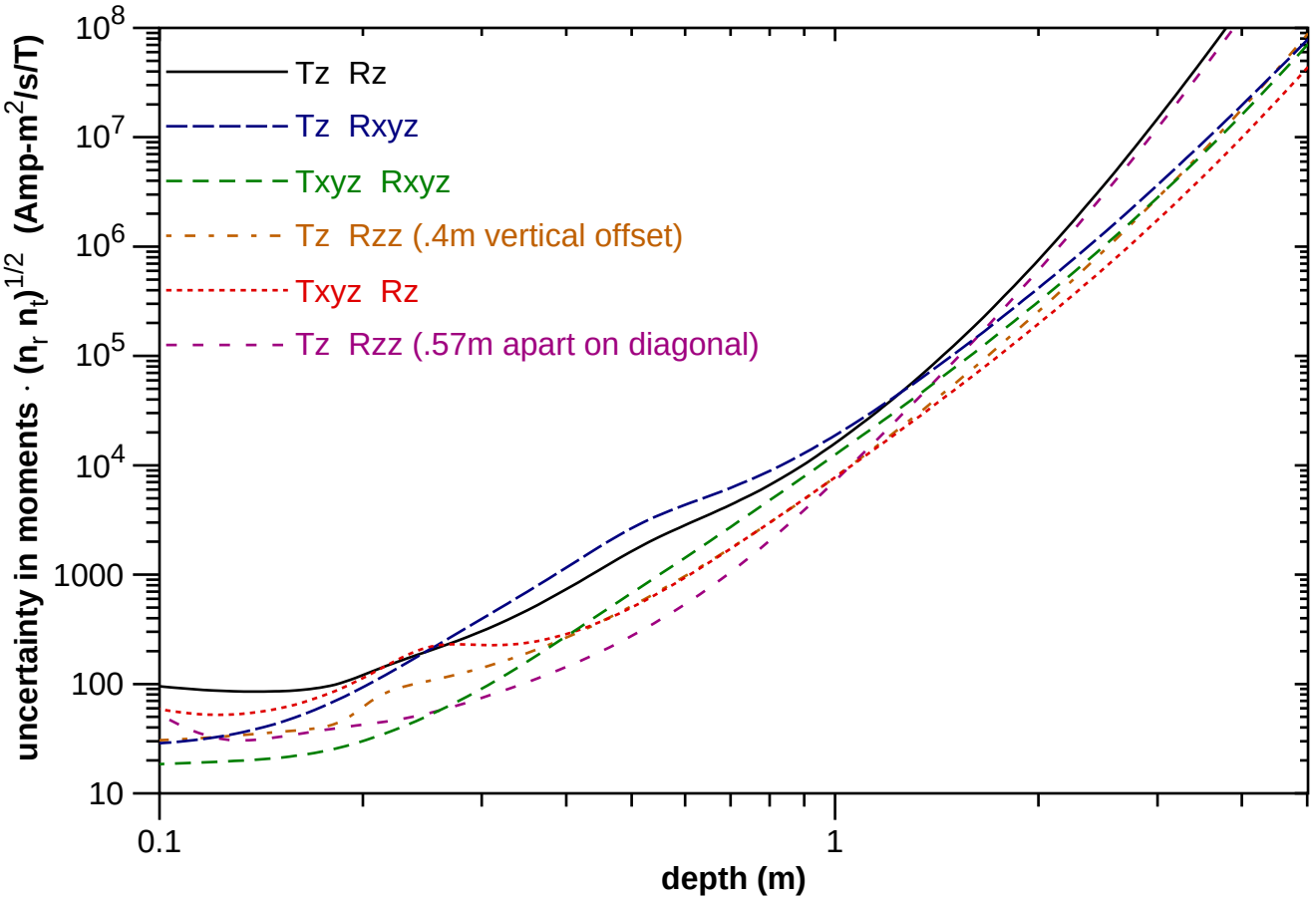
Tz Rz
Tz Rxyz
Txyz Rxyz
Tz Rzz (.4m vertical offset)
Txyz Rz
Tz Rzz (.57m apart on diagonal)
uncertainty in moments · (n_r n_t)^1/2 (Amp-m^2/s/T)
10^8
10^7
10^6
10^5
10^4
1000
100
10
0.1
1
depth (m)